G-Band Mode-Coupler-Based Si Dielectric Waveguide for Multidrop Sub-THz Interconnect

Xuan Ding[©], Member, IEEE, Hai Yu, Member, IEEE, Sajjad Sabbaghi, Graduate Student Member, IEEE, and Q. Jane Gu[©], Senior Member, IEEE

Abstract—This letter presents a G-band mode-coupler-based multimode Si dielectric waveguide (DWG) for multidrop sub-THz/THz interconnect. Three types of mode couplers, i.e., quasi-transverse electromagnetic (TEM) to E_{11}^y mode, E_{11}^y to E_{21}^y mode, and E_{11}^y to E_{31}^y mode, are designed and demonstrated. The quasi-TEM to E_{11}^y coupler works as microstrip line (MSL)-to-DWG transition. E_{11}^y to E_{21}^y and E_{11}^y to E_{31}^y mode couplers enable two more mode transmissions along the bus waveguide through the dedicated couplers where the phase match condition is satisfied. Tapers are used as the smooth transition between DWG sections, as well as mode filters to reduce the crosstalk between modes in (de)multiplexers. The measured minimum transition loss is about 5 dB with the 3-dB bandwidth of 143–200, 151–185, and 155–174 GHz for the three modes, respectively, and the measured crosstalk between modes is less than $-26~{\rm dB}$.

Index Terms—Communication, dielectric waveguide (DWG), E_{11}^y , E_{21}^y , E_{31}^y , G-band, interconnect, mode coupler, multidrop, nano-manufacturing, quasi-transverse electromagnetic (TEM), sub-THz, THz.

I. INTRODUCTION

CCORDING to Shannon–Hartley's theorem, channel bandwidth and transition loss, determining signal-to-noise ratio (SNR), are the key factors to limiting communication systems' data capacities. High-resistivity Si ($\varepsilon_r=11.7$, $\tan\delta=0.001$ [1]) dielectric waveguide (DWG)-based sub-THz/THz interconnect holds high potentials to address the long-standing challenge to satisfy ever-increasing data rate and energy efficiency requirements by leveraging the advantages of both electrical and optical interconnects, especially in the most challenging meter-range scenario [2].

Single-channel transmission in a waveguide has great advancements but is approaching the ceiling due to the constraint of active baseband circuits [3]. It is highly desired to adopt multiplexing schemes, such as frequency division multiplexing (FDM), coding division multiplexing (CDM), mode division multiplexing (MDM), and spatial division multiplexing (SDM), to make full use of the available bandwidth of waveguides, relieve the design burdens of active circuits,

Manuscript received 15 August 2022; revised 25 October 2022 and 2 January 2023; accepted 22 January 2023. Date of publication 2 February 2023; date of current version 7 June 2023. This work was supported in part by the U.S. National Science Foundation (NSF) and fabricated in part by the UC Davis Center for Nano and Micro Manufacturing (CNM2). (Corresponding author: Xuan Ding.)

The authors are with the Department of Electrical and Computer Engineering, University of California, Davis, CA 95616 USA (e-mail: xxding@ucdavis.edu; jgu@ucdavis.edu).

Color versions of one or more figures in this letter are available at https://doi.org/10.1109/LMWT.2023.3239624.

Digital Object Identifier 10.1109/LMWT.2023.3239624

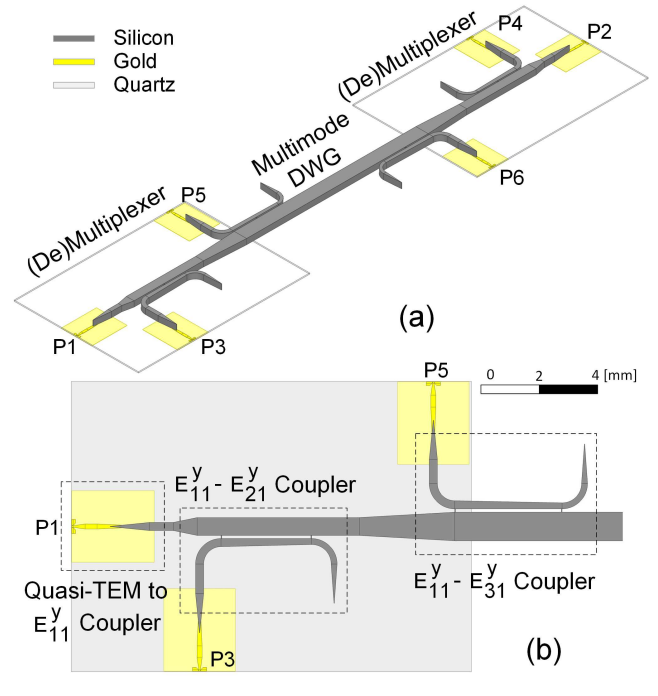


Fig. 1. (a) 3-D view of the new mode-coupler-based multimode Si DWG and (b) top view of mode couplers.

and further expand the data capacity of interconnect systems. (De)Multiplexer, a critical component in data links, is responsible for combining the channelized signal at the transmitter side and distributing signals correspondingly at the receiver side. It is required to have wide bandwidth to support high date rates, low loss to guarantee SNR, and high isolation to reject crosstalk. MDM [4], FDM [5], [6], [7], and SDM [8] multiplexers have been investigated and achieved competitive performances.

This letter presents a novel SDM (de)multiplexer based on three types of mode couplers. It is fabricated in-house with nano-manufacturing processes. The quasi-transverse electromagnetic (TEM) to E_{11}^y , E_{11}^y to E_{21}^y and E_{11}^y to E_{31}^y couplers are elaborated in Section II. To evaluate the idea, couplers are cascaded with bending and tapers and form the compact multiplexer, which allows three modes transmitting in the multimode Si DWG with less than -26-dB crosstalk for multidrop sub-THz/THz interconnect.

II. MULTIMODE SI DWG

The G-band mode-coupler-based multimode Si DWG is shown in Fig. 1(a), which is built with a multiplexer,

2771-957X © 2023 IEEE. Personal use is permitted, but republication/redistribution requires IEEE permission. See https://www.ieee.org/publications/rights/index.html for more information.

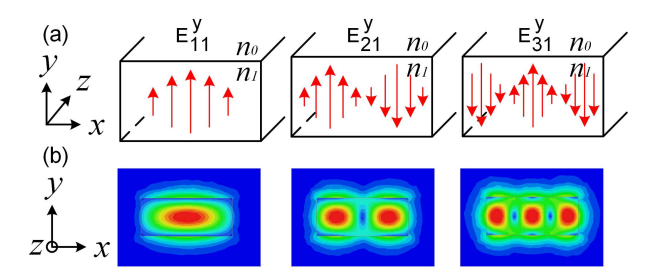


Fig. 2. E-field profiles of the E_{11}^y , E_{11}^y , and E_{31}^y modes in a multimode Si DWG with a height of 525 μm and a width of 1200 μm (a) vector and (b) magnitude.

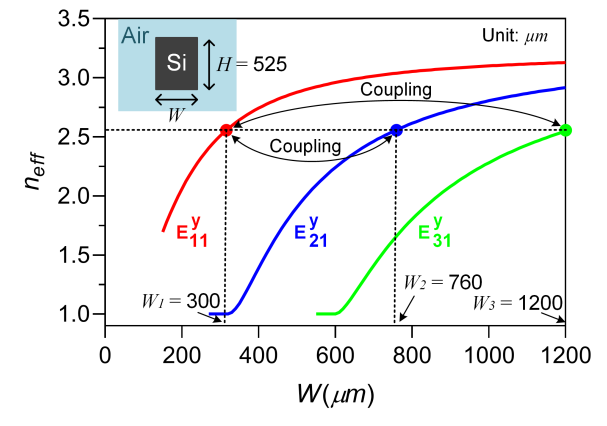


Fig. 3. Simulated effective refractive index n_{eff} for the three modes (E_{11}^y, E_{21}^y) , and (E_{31}^y) of a Si DWG versus width at 165 GHz.

multimode Si DWG, and demultiplexer on the other side. The bidirectional structure has six ports to excite and demultiplex E_{11}^y (P1 and P2), E_{21}^y (P3 and P4), and E_{31}^y (P5 and P6), respectively, and independently. Three types of mode couplers construct the (de)multiplexer, as shown in Fig. 1(b). Quasi-TEM to E_{11}^y mode coupler working as a microstrip line (MSL)-to-DWG transition is fabricated on the 100- μ m quartz. It generates and feeds E_{11}^y mode to all the ports of Si DWG. E_{11}^y to E_{21}^y and E_{11}^y to E_{31}^y mode couplers convert E_{11}^y into higher order modes at P3 and P5, and then three modes are generated, combined, and transmitted in the shared common waveguide in the center.

A. Multimode Si DWG Bus

The common section of the Si DWG should support multiple modes simultaneously. If only considering y-polarized modes, E_{11}^y , E_{21}^y , and E_{31}^y , whose E-field profiles are shown in Fig. 2, can exist together when the width of DWG is larger than 620 μ m, which is decided by the effective refractive index $n_{\rm eff}$ in Fig. 3. In other words, higher order modes, such as E_{21}^y and E_{31}^{y} , will be rejected or allowed in a DWG by simply reducing or increasing the waveguide width. This is similar as the operation principle of fiber mode filters to filter out undesired higher order modes [9]. For a rectangular Si core (refractive index $n_1 = 3.45$, cross-sectional area: $H \times W \mu m^2$) with air cladding (refractive index $n_0 = 1$), the n_{eff} and E-field profiles of all the eigen modes are determined and solved by the graphic approach [10] at a given frequency. The highest order mode determines the maximum number of modes that are supported by this DWG.

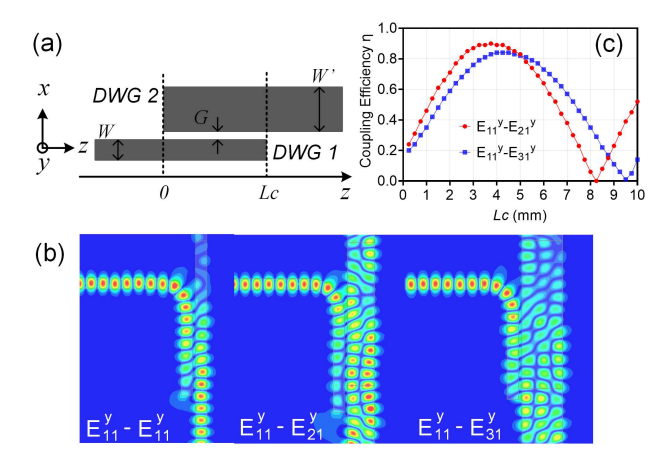


Fig. 4. (a) Design, (b) E-field distribution of the DWG mode coupler, and (c) simulated coupling efficiency versus the coupler length L_C at 165 GHz.

Bent DWG is widely used for structure integration, but small bending radius causes significant mode conversion and radiation leakage, thus introducing extra bending loss. Unwanted mode conversion is detrimental and leads to degradation in coupling efficiency and increase in crosstalk. According to the bending loss mechanism in [11], a smooth bending with a large radius is preferred to relieve the mode conversion and radiation issues. For the proposed triple-mode DWG, the bending radius should be larger than 1.4 mm and about 0.8-dB extra loss will be introduced by one bending.

B. E_{11}^y to E_{21}^y and E_{11}^y to E_{31}^y Couplers

The wave coupling can happen when the unshielded DWGs are close-by. Fig. 3 also describes the coupling mechanism between the same or different modes. The requirements for mode coupling include field overlap and phase matching. Field overlap means DWGs are close enough so that the EM field of each waveguide is interacting. Phase matching requires that the propagation constant β , which is the wavenumber along propagation direction, is equal for the coupling modes. By precisely controlling the width of DWG, $n_{\rm eff}$ of a specific mode can be finely tuned, and then it is possible to make two modes' phase matched according to (1).

$$\beta = n_{\text{eff}} \frac{\omega}{a} \tag{1}$$

where ω is the angular frequency, and c is the speed of light in vacuum. For example, at 165 GHz, $n_{\rm eff}$ of mode E_{11}^y in a DWG with $W_1 = 300~\mu{\rm m}$ is 2.55, which equals to $n_{\rm eff}$ of E_{21}^y in a DWG with $W_2 = 760~\mu{\rm m}$ and E_{31}^y in a DWG with $W_3 = 1200~\mu{\rm m}$.

Fig. 4(a) illuminates a DWG mode coupler with W and W' designed to align β of the specific modes as discussed. The coupling can be obtained between the same mode $(E_{11}^y \text{ to } E_{11}^y)$, or different modes $(E_{11}^y \text{ to } E_{21}^y \text{ and } E_{11}^y \text{ to } E_{31}^y)$, as shown in Fig. 4(b). The coupling coefficient κ exponentially decreases when the gap G of the coupler increases, because the field intensity exponentially decays out of the DWG. The coupling efficiency η defined by the energy coupled to the second DWG out of the total energy, which is optimized based on [12]

$$\eta = \frac{1}{1 + (\delta_{\beta}/\kappa)^2} \sin^2\left(\sqrt{\delta_{\beta}^2 + \kappa^2} z\right)$$
 (2)

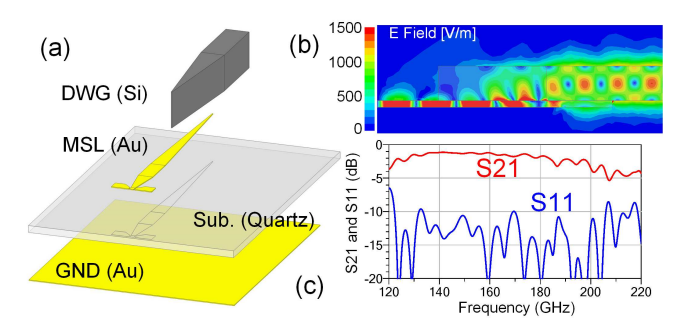


Fig. 5. (a) Configuration, (b) E-field distribution, and (c) simulated S-parameters of the quasi-TEM to E_{11}^y mode coupler.

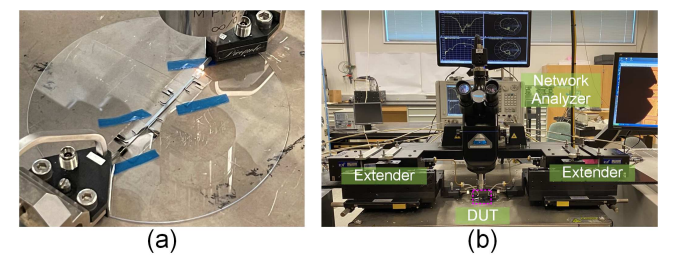


Fig. 6. Photograph of (a) complete multimode Si DWG and (b) measurement setup.

where $\delta_{\beta} = (\beta_1 - \beta_2)/2$ is the propagation constant difference, and z is the coupler length variable by assuming the DWGs start to overlap at z = 0. The maximum η occurs when

$$z = L_C = \frac{\pi}{\sqrt{\delta_{\beta}^2 + \kappa^2}} \left(m + \frac{1}{2} \right), \quad m = 0, 1, \dots, \infty.$$
 (3)

Then the coupling efficiency η reaches

$$\eta_{\text{max}} = \frac{1}{1 + (\delta_{\beta}/\kappa)^2}.$$
 (4)

In actual design, the first step is to minimize the propagation constant difference δ by tuning the width of DWG, and then select the optimum coupler length L_C . To reduce channel loss and reduce coupler size, the first peak point when m=0 is preferred. The simulated η along the propagation direction z is plotted in Fig. 4(c). $L_C=3.8$ mm for E_{11}^y to E_{21}^y coupler and $L_C=4.5$ mm for E_{11}^y to E_{31}^y coupler are selected.

C. Quasi-TEM to E_{11}^{y} Coupler

The configuration of the quasi-TEM to E_{11}^y coupler is shown in Fig. 5(a). It consists of a coplanar waveguide (CPW) interface with ac ground for ground-signal-ground (GSG) probe, oppositely tapered MSL and DWG to transit the electromagnetic wave smoothly. The quasi-TEM mode in MSL is gradually converted into E_{11}^y in DWG, as shown in Fig. 5(b). The structure is fabricated on a 100- μ m quartz ($\varepsilon_r = 3.78$, $\tan \delta = 0.0001$) substrate. The simulated S-parameters in Fig. 5(c) depict great transition performance.

III. FABRICATION AND MEASUREMENT RESULTS

The entire structure was modeled in the full-wave simulator HFSS and measured on-wafer with G-band (140–220 GHz) S-parameters' testbench. All the parts are fabricated in-house with the nano-manufacturing process. The multimode Si DWG and mode couplers are produced in one piece by the deep

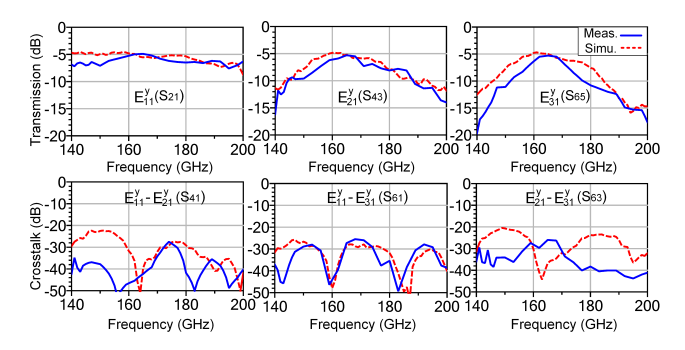


Fig. 7. Simulated and measured S-parameters of the entire multimode Si DWG including MSL-to-DWG transitions.

TABLE I Comparison With the SOA Multichannel Transmission Above 100 GHz

Ref.	2018 [4]	2020 [6]	2021 [7]	This Work
3-dB BW. (GHz)	150.8~206 151~171.4	$225 \sim 250^*$ $262 \sim 285^*$ $302 \sim 322^*$	127.7~152.3 168.3~191	143~200 151~185 155~174
Scheme	MDM	FDM	FDM	MDM
Tech.	DWG	Ridged SIW	MSL	DWG
No. CHNL.	2	3	2	3
Min Loss (dB)	6.4/6.6	6/8/10**	11.6/13.2	5/5.1/5.3
Crosstalk (dB)	-20	-35	-30	-26

* Read from the figure; ** the total loss of a multiplexer and demultiplexer.

reactive ion etching (DRIE) process. Quasi-TEM to E_{11}^y coupler with GSG interface is fabricated on a 100- μ m quartz substrate using lithography and metal deposition processes. The DWG and quartz substrate are assembled precisely by a flip-chip bonder to form the multiplexer structure. It is connected with 100- μ m pitch GSG pads, so it can be tested with commercial probes.

The measurement setup includes an Agilent network analyzer (PNA-X N5247A), a pair of Virginia Diodes frequency extension modules (VDI WR5.1-VNAX), WR-5 (140–220 GHz) S-bend waveguides, and a pair of WR-5 probes. The short, open, load, thru (SOLT) calibration method is used to set the reference plane at the probe tip. Fig. 6(b) shows the G-band S-parameters on-wafer testbench.

The simulated and measured *S*-parameters of the entire multimode Si DWG including MSL-to-DWG transitions are plotted in Fig. 7 and the results are compared with the state-of-the-art (SOA) multichannel transmission over 100-GHz carriers in Table I. The minimum loss is about 5 dB within the 3-dB bandwidth of 143–200, 151–185, and 155–174 GHz, respectively, for the three modes. The measured crosstalk between modes is less than –26 dB. The comparison with SOAs above 100 GHz reveals that the proposed approach achieves competitive loss and bandwidth performances.

IV. CONCLUSION

This letter presents a mode-coupler-based multimode Si DWG in the G-band with the design, analysis, and demonstration elaborated. This is the first time three-MDM-based channelization is demonstrated on a DWG. The design method can be extended to more modes and opens a new direction to more efficiently use the extremely broad bandwidth of DWG to materialize high bandwidth density and high energy efficiency multidrop sub-THz/THz interconnect to meet the ever-increasing interconnect demands.

REFERENCES

- [1] B. Yu et al., "Sub-THz interconnect for planar chip-to-chip communications," in *Proc. IEEE 18th Top. Meeting Silicon Monolithic Integr. Circuits RF Syst. (SiRF)*, Jan. 2018, pp. 54–56.
- [2] Q. J. Gu, B. Yu, X. Ding, Y. Ye, X. Liu, and Z. Xu, "THz interconnect for inter-/intra-chip communication," *Proc. SPIE*, vol. 10982, May 2019, Art. no. 109822R.
- [3] Q. J. Gu, "Sub-THz/THz interconnect, complement to electrical and optical interconnects: Addressing fundamental challenges related to communication distances," *IEEE Solid StateCircuits Mag.*, vol. 12, no. 4, pp. 20–32, Fall 2020.
- [4] B. Yu et al., "Ortho-mode sub-THz interconnect channel for planar chip-to-chip communications," *IEEE Trans. Microw. Theory Techn.*, vol. 66, no. 4, pp. 1864–1873, Apr. 2018.
- [5] S. Fukuda et al., "A 12.5+12.5 Gb/s full-duplex plastic waveguide interconnect," *IEEE J. Solid-State Circuits*, vol. 46, no. 12, pp. 3113–3125, Dec. 2011.
- [6] J. W. Holloway, G. C. Dogiamis, S. Shin, and R. Han, "220-to-330-GHz manifold triplexer with wide stopband utilizing ridged substrate integrated waveguides," *IEEE Trans. Microw. Theory Techn.*, vol. 68, no. 8, pp. 3428–3438, Aug. 2020.

- [7] X. Ding, B. Yu, Y. Ye, H. Yu, Z. Xu, and Q. Jane Gu, "An FDD-based full-duplex sub-THz interconnect with data-rate of 22.6 Gb/s and energy-efficiency of 1.58 pJ/bit," in *Proc. 46th Int. Conf. Infr., Millim. Terahertz Waves (IRMMW-THz)*, Aug. 2021, pp. 1–2.
- [8] H.-I. Song et al., "A 50 Gb/s PAM-4 bi-directional plastic waveguide link with carrier synchronization using PI-based Costas loop," in *IEEE Int. Solid-State Circuits Conf. (ISSCC) Dig. Tech. Papers*, vol. 65, Feb. 2022, pp. 1–3.
- [9] S. Moon and D. Y. Kim, "Effective single-mode transmission at wavelengths shorter than the cutoff wavelength of an optical fiber," *IEEE Photon. Technol. Lett.*, vol. 17, no. 12, pp. 2604–2606, Dec. 2005.
- [10] S. Chuang, Physics of Photonic Devices (Wiley Series in Pure and Applied Optics). Hoboken, NJ, USA: Wiley, 2009.
- [11] R. Hunsperger, Integrated Optics: Theory Technol. (Advanced Texts in Physics). New York, NY, USA: Springer, 2009.
- [12] K. Okamoto, Fundamentals of Optical Waveguides. Amsterdam, The Netherlands: Elsevier, 2021.